ELSEVIER

Journal of Power Sources 112 (2002) 216–221

JOURNAL OF POWER SOURCES

www.elsevier.com/locate/jpowsour

# Electrochemical insertion of lithium into multi-walled carbon nanotubes prepared by catalytic decomposition

Heon-Cheol Shin[a], Meilin Liu[a,*], B. Sadanadan[b], Apparao M. Rao[b]

[a]*School of Materials Science and Engineering, Georgia Institute of Technology, Atlanta, GA 30332-0245, USA*
[b]*Kinard Laboratory of Physics, Clemson University, Clemson, SC 29634, USA*

Received 20 June 2002; accepted 27 June 2002

**Abstract**

Various electrochemical techniques have been used to study the electrochemical insertion (extraction) of lithium into (from) multi-walled carbon nanotubes (MWNTs) prepared by catalytic decomposition of ferrocene and xylene. The galvanostatic charge/discharge profiles display a small hysteretic loss and the cyclic voltammograms are quite symmetric in the shape of cathodic and anodic branches, implying that lithium insertion/extraction process is highly reversible. In addition, rate capability and cycleability of charge into the MWNTs are satisfactory. The excellent reversibility and small hysteretic loss of the MWNT are attributed to the extremely pure structural character of the MWNTs with moderate chemical diffusion coefficient of lithium through the structure.


*Keywords:* Carbon nanotube; Catalytic decomposition; Lithium battery

## 1. Introduction

The rapid advancements in microelectronic and telecommunication devices such as cellular phones, laptop computers and portable cameras demand a new generation of rechargeable lithium battery with high-performance. The key to successful development of high-performance lithium batteries depends critically on the creation or identification of new electrode and electrolyte materials that offer high energy and power density, long shelf and cycle life, low-cost, and a minimal probability for environmental disposal problems.

To date, much effort has been devoted to the development of novel anode materials with excellent rechargeability and minimal capacity fade. In particular, carbon-based materials, including carbon nanotubes, have attracted much attention. Their one-dimensional structure with a central core may allow rapid intercalation/deintercalation of lithium into/from the nanotubes [1–5].

In this communication, we report the electrochemical properties of multi-walled carbon nanotubes (MWNTs) prepared by catalytic decomposition of ferrocene and xylene. Since the MWNTs are synthesized under atmospheric pressure at moderate temperatures without any preformed substrate, a large amount of pure MWNT can be readily produced cost effectively. The hysteretic loss, cycleability, and rate capability will be compared with those of the MWNTs reported previously. Further, the diffusivity of lithium in the MWNTs will be presented.

## 2. Experimental

### 2.1. Specimen preparation

High-purity MWNT samples were prepared through catalytic decomposition of ferrocene–xylene mixture as described elsewhere [6]. The process is briefly summarized as follows: ~6.5 mol% of ferrocene was dissolved in xylene and was fed continuously into a two-stage tubular quartz reactor. The liquid feed is first passed through capillary tube and preheated ~200 °C. At this temperature, the liquid is immediately volatilized and the volatized mixture is swept into the reaction zone of the furnace by a flow of argon with 10% hydrogen. Decomposition of ferrocene–xylene mixture in the reaction zone gave us the nanotubular carbon deposit. Electron microscopy studies revealed the MWNTs to be of high-purity without the presence of amorphous carbons [6].

### 2.2. Electrochemical test

A three-electrode electrochemical cell was employed for all electrochemical measurements using lithium foils as the

* Corresponding author. Tel.: +1-404-894-6114; fax: +1-404-894-9140.
*E-mail address:* meilin.liu@mse.gatech.edu (M. Liu).

0378-7753/02/$ – see front matter 
PII: S0378-7753(02)00366-X

counter and reference electrode. The working electrode was composed of MWNT (85 wt.%), carbon black (5 wt.%), and polyvinylidene fluoride (PVDF) binder (10 wt.%). The mixture was prepared by ball milling and the slurry was cast on Ni plate, followed by drying at 180 °C in vacuum for 24 h and uniaxial pressing between 2 flat plates at ~500 psi for 5 min. A Celgard 2500 separator, wetted with 1 M solution of $LiPF_6$ in a 50/50 (v/o) mixture of ethylene carbonate (EC) and diethyl carbonate (DEC), was sandwiched between a MWNT working electrode and a lithium counter electrode. All cells were assembled and tested in a glove box filled with purified argon gas. Lithium transport behavior through the MWNT was characterized using a potentiostatic intermittent titration technique (PITT) [7] and galvanostatic method [8]. PITT was performed at a voltage scan rate of 50 mV $h^{-1}$ between 3.0 and 0.5 V (versus $Li/Li^+$) and of 10 mV $h^{-1}$ between 0.5 and 0.03 V (versus $Li/Li^+$).

## 3. Results and discussion

### 3.1. Capacity and reversibility

Shown in Fig. 1(a) are the charge–discharge curves of an MWNT/Li cell at a current density of 50 mA $g^{-1}$ carbon MWNTs for the first 3 cycles. After the first discharge process, lithium insertion (extraction) into (from) the MWNT is nearly reversible. The reversible capacities of the MWNT/Li cells are comparable to those reported in the literature [1–3], varying from 200 to 250 mAh $g^{-1}$. In our cycling tests, however, the current density (50 mA $g^{-1}$) was higher than those used in previous studies (15–40 mA $g^{-1}$ [1–3]). It is expected that the reversible capacity should be higher at a lower current density. Further, the hysteretic behavior, i.e. the difference between the potential of lithium insertion and that of lithium extraction, is significantly improved as compared to those reported previously [1–3]. For example, about 130 mAh $g^{-1}$ (more than 60% of the reversible capacity) is gathered below 0.5 V (versus $Li/Li^+$) during lithium extraction. The small hysteresis loss is due probably to the fact that the MWNT is extremely pure, free of amorphous carbon, as determined from HRTEM images of MWNT samples [6].

Shown in Fig. 1(b) are differential capacities (d$C$/d$E$) versus cell voltages, an effective way of describing the charge/discharge behavior. The differential capacity curve derived from the first discharge curve showed 2 distinct peaks at about 0.6 and 0.8 V (versus $Li/Li^+$), which correspond to the decomposition of the electrolyte and the formation of a solid electrolyte interphase (SEI) layer [1,9]. The origin of the additional small but broad peak at ca. 2.2 V (versus $Li/Li^+$) is still not clear, although it may correspond to the reduction of oxygenated species [1] at ca. 2.2 V (versus $Li/Li^+$). Since the open circuit voltage (OCV) of the MWNT/Li cell was higher than 3.0 V (versus $Li/Li^+$) before the very first charge/discharge experiment, it is likely

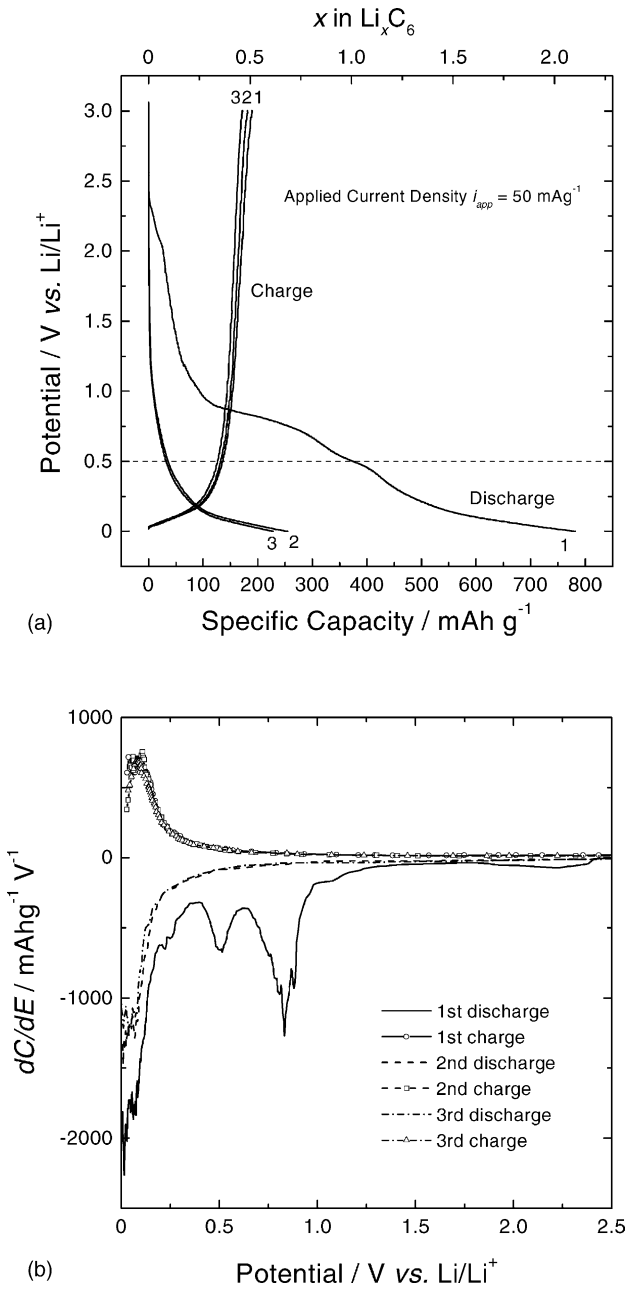


Fig. 1. (a) Charge–discharge curves and (b) their differential capacity vs. voltage plots obtained from the MWNT in a 1 M $LiPF_6$-EC/DEC solution at a current density of 50 mA $g^{-1}$ carbon MWNT.

that some oxygenated species are present [1]. In subsequent cycles, the 3 peaks were hardly observable: d$C$/d$E$ versus $E$ plots were characterized only by high absolute values of d$C$/d$E$ below 0.5 V (versus $Li/Li^+$) due to lithium insertion/extraction. It is also noted that, except for the first discharge, the differential capacities (d$C$/d$E$) for subsequent charge and discharge processes were nearly identical, an indication of good reversibility during cycling.

The excellent reversibility and small hysteresis loss can be better illustrated with the cyclic voltammograms for the MWNT samples. Fig. 2(a) depicts the cyclic voltammograms

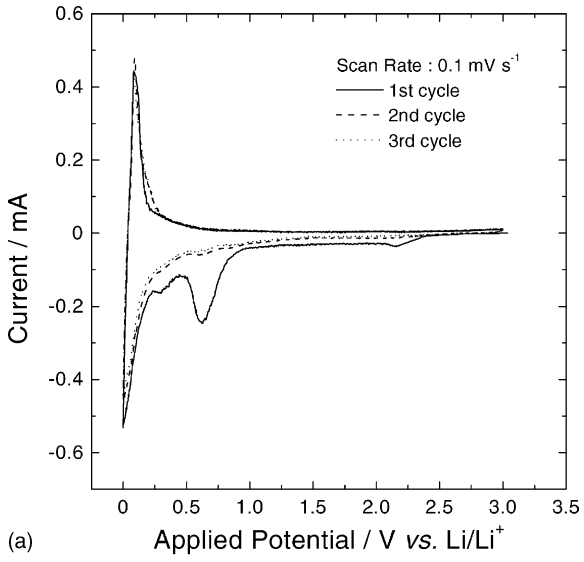


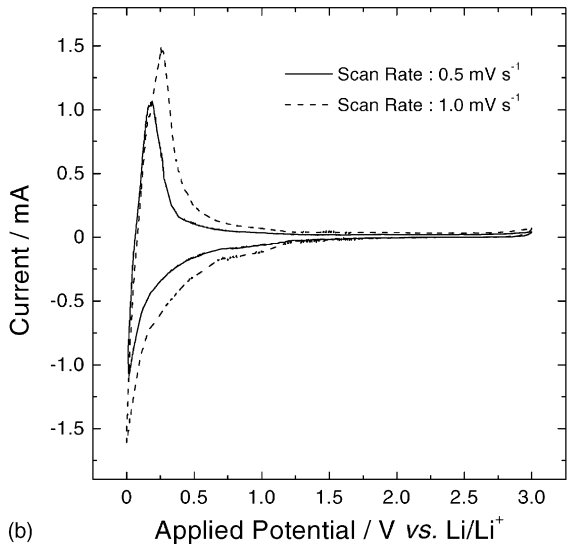


Fig. 2. Cyclic voltammograms obtained from the MWNT in a 1 M $LiPF_6$-EC/DEC solution at a scan rate of (a) 0.1 mV $s^{-1}$ for the first 3 cycles and (b) 0.5 and 1.0 mV $s^{-1}$ after 5 cycles.

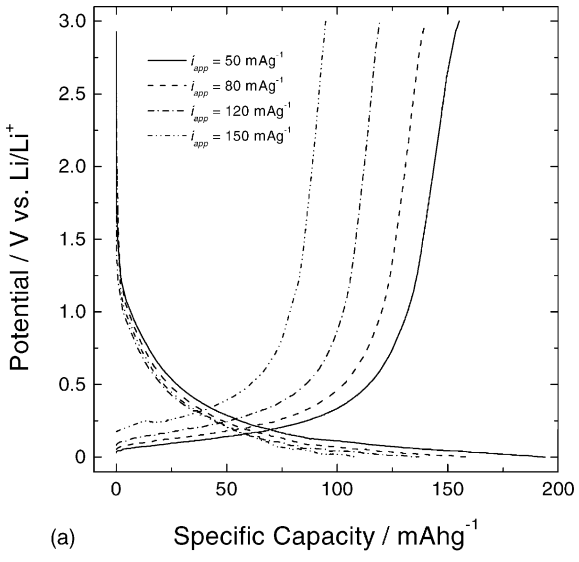


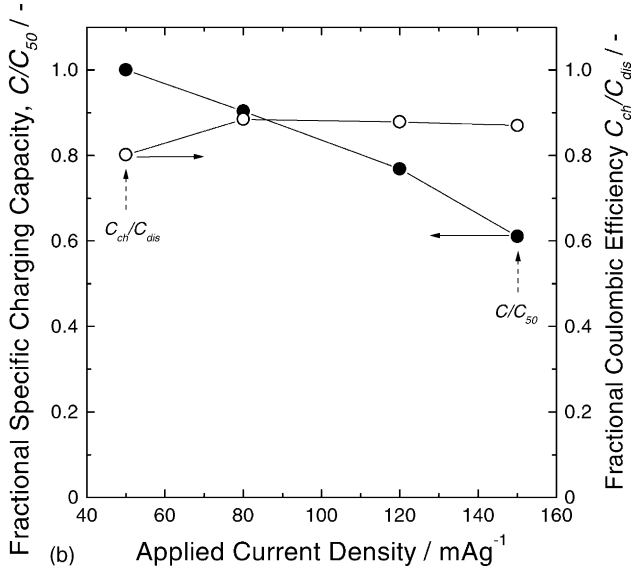


Fig. 3. (a) Charge–discharge curves obtained from the MWNT in a 1 M $LiPF_6$-EC/DEC solution at different applied current densities and (b) the variations in fractional specific charging capacity and fractional coulombic efficiency with applied current density, reconstructed from Fig. 3(a).

at a scan rate of 0.1 mV $s^{-1}$ for the first 3 cycles. There are three irreversible peaks in the cathodic branch of the first cyclic voltammogram, which is consistent with the charge/discharge behavior of Fig. 1(a) and (b). But, the locations of the corresponding peaks in the cyclic voltammograms are slightly shifted in the cathodic direction due to the effect of ohmic resistance. It is noted that the shape of cathodic and anodic branches, corresponding to lithium insertion and extraction, respectively, is nearly symmetric at a scan rate of 0.1 mV $s^{-1}$. Furthermore, the symmetrical feature is also evident at relatively high scan rates (0.5 and 1.0 mV $s^{-1}$), as can be seen in Fig. 3(b). These characteristics are a strong indication that the lithium insertion and extraction are highly reversible.

In comparison to the MWNTs for Li batteries reported in the literature, the MWNT samples exhibit much better reversibility. Further, the MWNT can be produced cost-effectively since the synthesis of our MWNT does not require a preformed substrate and can be produced under atmospheric pressure at moderate temperatures. Accordingly, the MWNT could be a low-cost, high-performance anode material for rechargeable lithium-ion batteries. It is this superior reversibility that encouraged us to further investigate the rate capability, cycleability, and the kinetics of lithium insertion.

Shown in Fig. 3(a) are the voltage profiles of MWNT (versus $Li/Li^+$) obtained at different current densities: 50, 80, 120, and 150 mA $g^{-1}$. At a very high charging rate of

150 mA $g^{-1}$, MWNT exhibited above 60% of charging capacity retention. As expected, the overvoltage increases with increasing current density, leading to a decreased capacity at a given cut-off voltage during cycling. This is confirmed by the observation that the fractional coulombic efficiency, i.e. the ratio of the amount of transferred charge during discharging process to that during subsequent charging process, remained at about 0.9, irrespective of applied current density, as shown in Fig. 3(b). These results indicate that the reversible charge/discharge character remained even at very high cycling rates. Fig. 4 presents variations in fractional charging capacity retention with the number of cycles at a current density of 50 mA $g^{-1}$. Apart from the irreversible capacity fade during the initial 5 cycles, there is little capacity fade during subsequent 80 charge–discharge cycles.

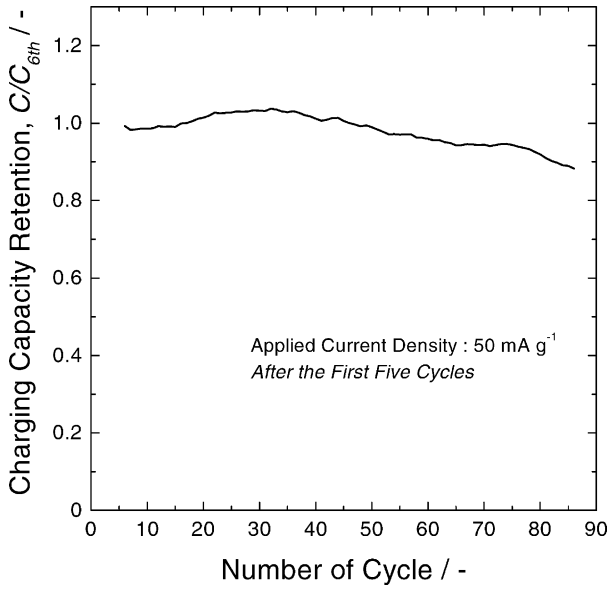


Fig. 4. Dependence of charging capacity retention of the MWNT on the number of cycle at a constant current of 50 mA $g^{-1}$ carbon MWNT.

### 3.2. Lithium ion diffusivity

Shown in Fig. 5 are typical chronoamperometric curves obtained from the MWNT at a potential region below 0.5 V (versus $Li/Li^+$). At the same time, in order to explore the diffusion behavior of lithium inside the MWNT during potential stepping, the corresponding $It^{1/2}$ versus log $t$ plots were reconstructed from the chronoamperometric curves. If there is a plateau region (i.e. Cottrell region) in the $It^{1/2}$ versus log $t$ plots in a short time range, the PITT can be effectively used to investigate the lithium diffusion behavior.

Unfortunately, there is no Cottrell region throughout the entire lithium insertion region. This behavior in intercalation compounds has been discussed elsewhere [10–12]. In particular, Montella suggested [12] that no Cottrell region is observed in case that the value of interfacial resistance is significant as compared to diffusional resistance. It was further implied [12] that the chemical diffusion coefficients may have been significantly underestimated assuming that the shallow local maximum on the $It^{1/2}$ versus log $t$ plot corresponded to the Cottrell region [13–15]. Our MWNT is likely to be controlled by slow interfacial reaction during the

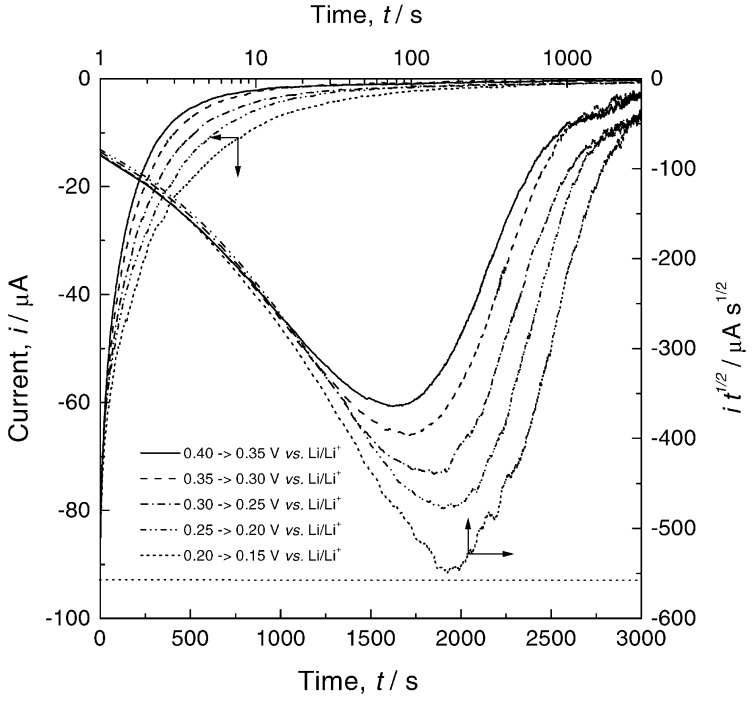


Fig. 5. Current responses of the MWNT to different applied potential steps.

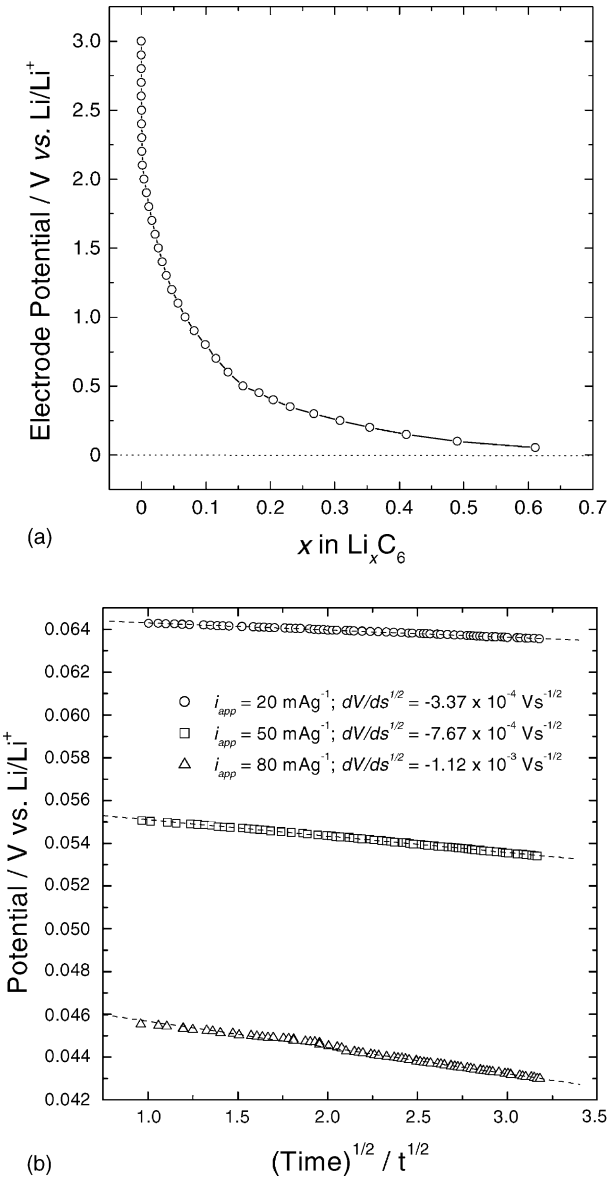


Fig. 6. (a) Coulometric titration curve of MWNT and (b) dependence of potential on square root of time at different current pulses for estimating the chemical diffusion coefficient of lithium in the MWNT.

chronoamperometric measurements. The exact mechanism of lithium insertion into the MWNT under these conditions is still under investigation.

Under the circumstances, we are unable to use the PITT to determine the chemical diffusion coefficient of lithium. Instead, we adopted a galvanostatic approach. From the titration curve of MWNT and the potential response to current pulse in a short time range, the chemical diffusion coefficient of lithium inside the MWNT can be determined as follows [8],

$$\tilde{D} = \frac{4}{\pi}\left(\frac{IV_{\mathrm{M}}}{FS}\right)^2\left[\frac{(\mathrm{d}E/\mathrm{d}x)}{(\mathrm{d}E/\mathrm{d}\sqrt{t})}\right]^2, \quad t \ll \frac{L^2}{\tilde{D}}$$

where $\tilde{D}$ is the chemical diffusion coefficient of lithium in the MWNT; $I$ the applied current; $V_{\mathrm{M}}$ the molar volume of the MWNT; $F$ the Faraday constant; $S$ the surface area of the MWNT; $\mathrm{d}E/\mathrm{d}x$ the slope of the coulometric titration curve, and $\mathrm{d}E/\mathrm{d}\sqrt{t}$ represents the slope of potential versus square root of time during current pulse. Especially, $\mathrm{d}E/\mathrm{d}x$ was estimated from the titration curve obtained from the PITT measurements, as shown in Fig. 6(a). It is assumed that the molar volume $V_{\mathrm{M}}$ of the MWNT is similar to that of graphite (5.29 $\mathrm{cm^3\ mol^{-1}}$) and surface area of the electrode $S$ is the superficial geometrical area of the electrode (0.25 $\mathrm{cm^2}$).

Shown in Fig. 6(b) are the dependences of potential on square root of time in a short time range at different values of current pulse. The OCV prior to applying current pulse was 0.07 V (versus $\mathrm{Li/Li^+}$), independent of the applied current density. All three curves can be well approximated by a straight line, as suggested by a linear regression analysis. The chemical diffusion coefficient of lithium in the MWNT is estimated to be $3 \times 10^{-11}$ $\mathrm{cm^2\ s^{-1}}$. Since a wide range of diffusion coefficient of lithium has been reported for typical graphitized carbon, ranging from $10^{-8}$ to $10^{-11}$ $\mathrm{cm^2\ s^{-1}}$ [16–19], the direct comparison of the diffusion coefficient of the MWNT with those of other graphitized carbons is very difficult. Nevertheless, it is noticeable that the diffusion coefficient of lithium in the MWNT falls within the range of that of graphitized carbon. High-purity of the MWNT with moderate rate of lithium diffusion is thought to be responsible for the excellent reversibility and rate capability of our MWNT.

## 4. Conclusions

The MWNT, prepared by catalytic decomposition of ferrocene and xylene, exhibits very small hysteresis loss during lithium insertion and extraction with excellent reversible capacity and cycleability. In addition, the chemical diffusion coefficient of lithium in the carbon nanotubes was comparable to that in graphite. The MWNT could be a low-cost, high-performance anode material for rechargeable lithium-ion batteries.

## Acknowledgements

This work was supported by Office of Science, Department of Energy under Grant No. DE-FG02-01ER15220. One of the authors (Heon-Cheol Shin) would also like to acknowledge the partial support by the Post-doctoral Fellowship Program of Korea Science & Engineering Foundation (KOSEF). Apparao M. Rao acknowledges support for this work from a grant through NASA Ames Research Center.

## References

[1] E. Frackowiak, S. Gautier, H. Gaucher, S. Bonnamy, F. Beguin, Carbon 37 (1999) 61.
[2] B. Gao, A. Kleinhammes, X.P. Tang, C. Bower, L. Fleming, Y. Wu, O. Zhou, Chem. Phys. Lett. 307 (1999) 153.

[3] G.T. Wu, C.S. Wang, X.B. Zhang, H.S. Yang, Z.F. Qi, P.M. He, W. Z Li, J. Electrochem. Soc. 146 (1999) 1696.
[4] A.S. Claye, J.E. Fischer, C.B. Huffman, A.G. Rinzler, R.E. Smalley, J. Electrochem. Soc. 147 (2000) 2845.
[5] H. Shimoda, B. Gao, X.P. Tang, A. Kleinhammes, L. Fleming, Y. Wu, O. Zhou, Phys. Rev. Lett. 88 (2002) 015502.
[6] R. Andrews, D. Jacques, A.M. Rao, F. Derbyshire, D. Qian, X. Fan, E.C. Dickey, J. Chen, Chem. Phys. Lett. 303 (1999) 467.
[7] C.J. Wen, B.A. Boukamp, R.A. Huggins, W. Weppner, J. Electrochem. Soc. 126 (1979) 2258.
[8] W. Weppner, R.A. Huggins, J. Electrochem. Soc. 124 (1977) 1569.
[9] D. Aurbach, Y. Ein-Eli, J. Electrochem. Soc. 142 (1995) 1746.
[10] H.-C. Shin, S.-I. Pyun, Electrochim. Acta 45 (1999) 489.
[11] J.J. Garcia-Jareño, A. Sanmatías, J. Navarro-Laboulais, F. Vicente, Electrochim. Acta 44 (1999) 4753.
[12] C. Montella, J. Electroanal. Chem. 518 (2002) 61.
[13] B. Markovsky, M.D. Levi, D. Aurbach, Electrochim. Acta 43 (1998) 2287.
[14] W. Yang, G. Zhang, S. Lu, J. Xie, Q. Liu, Solid State Ionics 121 (1999) 85.
[15] F. Varsano, F. Decker, E. Masetti, F. Croce, Electrochim. Acta 46 (2001) 2069.
[16] J.M. Tarascon, D. Guyomard, J. Electrochem. Soc. 139 (1992) 937.
[17] M. Morita, N. Nishimura, Y. Matsuda, Electrochim. Acta 38 (1993) 1721.
[18] M.D. Levi, D. Aurbach, J. Phys. Chem. B 101 (1997) 4641.
[19] P. Yu, B.N. Popov, J.A. Ritter, R.E. White, J. Electrochem. Soc. 146 (1999) 8.